Electrochemical Behavior of Graphite–Lithium Intercalation Electrode in $AlCl_3$–EMIC–LiCl–$SOCl_2$ Room-Temperature Molten Salt

Nobuyuki Koura, * Keiko Etoh, Yasushi Idemoto, and Futoshi Matsumoto
Faculty of Science and Technology, Tokyo University of Science, 2641 Yamazaki, Noda, Chiba 278-8510

(Received August 8, 2001; CL-010742)

The electrochemical behavior of a graphite (comprising only artificial graphite particles) electrode for intercalation and deintercalation of Li^+, in $AlCl_3$–1-ethyl-3-methylimidazolium chloride (EMIC)–LiCl–thionyl chloride ($SOCl_2$) melt was studied.

The improvement in the energy density of rechargeable batteries, employing a carbon–lithium intercalation anode, a transition metal oxide intercalation cathode, and organic solvents containing Li salts is investigated by many groups. Development of high-powered lithium secondary batteries progresses rapidly. At the same time, the issue of safety in lithium secondary batteries, especially against ignition and inflammation, with increasing in the energy density is the major problem to be solved. Room-temperature molten salts composed of $AlCl_3$, EMIC, and LiCl, recently have been investigated extensively as electrolytes for Li secondary batteries because these melts have several unique properties for the development of lithium secondary batteries with higher safety and performance, such as a wide electrochemical window, high inherent conductivity, negligible vapor pressure, and nonflammability.[1–3] However, the operation of a carbon–lithium intercalation anode in the room-temperature molten salt has not been reported. We examined the Li^+ intercalation–deintercalation processes into and from a binder-free graphite electrode (artificial graphite : KS-25 (Timcal)), which is fabricated using electrophoretic deposition (EPD) method,[4] in the $AlCl_3$–EMIC–LiCl–$SOCl_2$ melt and report firstly the occurrence of the Li^+ intercalation–deintercalation into and from a artificial graphite in the room-temperature molten salt.

$AlCl_3$–EMIC melt was prepared as previously reported. The melt (colorless liquid) was purified using Al substitution method.[3] Anhydrous LiCl dried under vacuum at 200 °C for one week was added to the melt. The addition of purified $SOCl_2$ into the $AlCl_3$–EMIC–LiCl melt extended an electrochemical window as far as Li can be deposited.[2] All experiments were performed under a purified Ar atmosphere in a Vaccum Atmosphere's dry box. The EPD bath was prepared by suspending an artificial graphite (5 $g \cdot L^{-1}$) and triethylamine (1 $mL \cdot L^{-1}$) in acetonitrile using an ultrasonic clearner. The anode and cathode substrates were Mo and Pt, respectively. The deposition of graphite particles was done at 300 V for 30 s. Graphite particles covered uniformly the Mo current collector surface (1.8 $mg \cdot cm^{-2}$) and its thickness was 60 μm.

Figure 1 shows typical cyclic voltammogram obtained with a binder-free graphite electrode in the LiCl-saturated $AlCl_3$ (60 mol%)–EMIC (40 mol%) melt containing 0.11 $mol \cdot dm^{-3}$ $SOCl_2$ at 0.2 mVs^{-1}. Irreversible reduction peak current was observed at 2.8 V(vs Li / Li^+) and smaller reduction current was observed in the potential region from 0.3 to 2.5 V at the first cycle. With the following potential scan, these reduction currents decreased. Moreover, in the potential region from 0 to 0.2 V, three coupled redox peaks were observed and these peak currents reached a steady-state after the 5th cycle. When the electrode potential was held at 15 mV, the electrode surface exhibited a golden-yellow color. The electrochemical behavior in the potential region from 0 to 0.2 V was very similar to the one observed in EC–DMC (ethylenecarbonate–dimethylcarbonate)(1:3) / $LiAsF_6$ with a graphite–lithium intercalation electrode comprising artificial graphite and binder ((polyvinylidene fluoride) (PVDF)).[5] It is well-known that representative three coupled redox peaks, indicating the phase transitions between Li^+ intercalation stages, were observed in organic solvent containing Li salt. The first, second, and third stages were identified as a stage for the formation of the structure composed of LiC_6, $Li_{0.5}C_6$, and $Li_{0.16}C_6$, respectively. A surface of graphite electrode intercalated stepwise to LiC_6 shows a golden-yellow color.[6] In comparison with the results obtained from the graphite electrode, comprising artificial graphite and PVDF, in organic solution, it can be postulated that the intercalation and deintercalation of Li^+ into and from the binder-free graphite electrode occur in the $AlCl_3$–EMIC–LiCl–$SOCl_2$ melt. Moreover, the reduction peak current observed at 2.8 V at the first potential scan can be assigned to the reduction of $SOCl_2$.[7] The reduction current observed in the potential region from 0.3 to 2.5 V may be due to the formation of the surface electrolyte interphase (SEI).

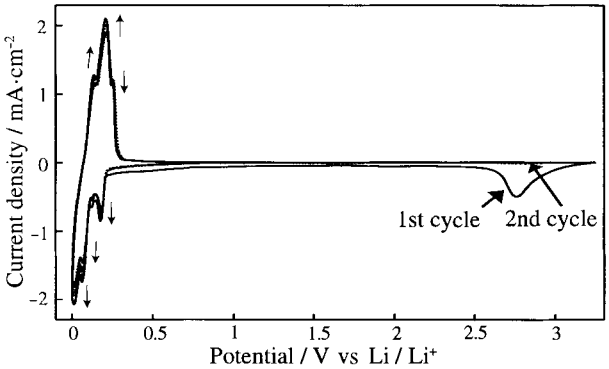

Figure 1. Typical voltammetric behavior of a binder-free graphite electrode at 0.2 $mV \cdot s^{-1}$ in the LiCl-saturated $AlCl_3$ (60 mol%)-EMIC(40 mol%) melt containing 0.11 $mol \cdot dm^{-3}$ $SOCl_2$. The binder-free graphite electrode was prepared with artificial graphite (KS-25, 1.8 $mg \cdot cm^{-2}$ on Mo). Electrolyte temp.: 20 ℃

In order to confirm the structural change after the reductive Li^+ intercalation, X-ray diffraction (XRD) was carried out at the binder-free graphite electrode reduced until the first stage (LiC_6). Figure 2 shows the XRD data obtained with the electrode before and after the reduction. The XRD pattern measured with the binder-free graphite electrode before the reduction shows a highly crystalline graphite and clear (001) and (002) diffraction peaks were observed (Figure 2(a)).[6,8] After the reduction, these peaks shifted to lower degree and it indicates an

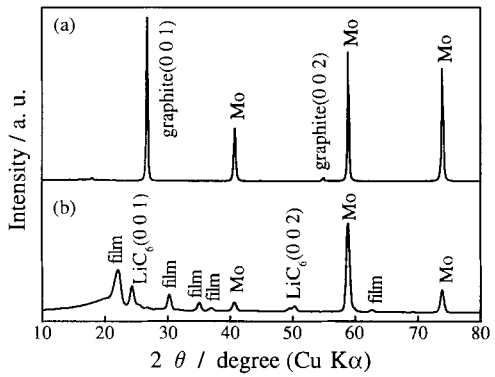

Figure 2. XRD spectra of the binder-free graphite electrode (artificial graphite, KS-25, 1.8 mg·cm^{-2} on Mo) before (a) and after (b) the potential was held at 15 mV for 60 min in the $AlCl_3$–EMIC–LiCl–$SOCl_2$ melt. In measuring XRD data, the electrode after the reduction was covered with a polyethylene film.

increase in the distance between the graphite layers due to the Li^+ intercalation (Figure 2(b)).

Representative intercalation–deintercalation cycling of Li^+ obtained with the binder-free graphite electrode at constant-current electrolysis in the LiCl-saturated $AlCl_3$ (60 mol%)–EMIC(40 mol%) melt containing 0.11 mol·dm^{-3} $SOCl_2$ are shown in Figures 3 and 4. The reduction was done at the first cycle in the rate of 0.5 C (0.28 mA·cm^{-2}). The following reduction and oxidation were done in the rate of 0.2 C. A potential vs reduction capacity curve (Figure 3) at the first cycle was quite different from those at the following cycles. The curve was composed of several sloping and plateau regions and showed the electrode potentials from 0 to 2.5 V. The reason for the appearance of higher potential than one for the intercalation of Li^+ is that the applied constant current is consumed by the reduction of $SOCl_2$ and the formation of the SEI. In the case of the lower reduction rate than 0.5 C at first cycle, the electrode potential was kept at the reduction potential of $SOCl_2$. The reduction capacity at the first cycle exceeded the theoretical capacity of graphite (327 mAh·g^{-1}) and reached 750 mAh·g^{-1} (Figure 3, solid line). The excess of the reduction capacity at the first cycle is due to the additional capacity of the $SOCl_2$ reduction and the SEI formation. Therefore, the oxidation capacity at the first cycle is only

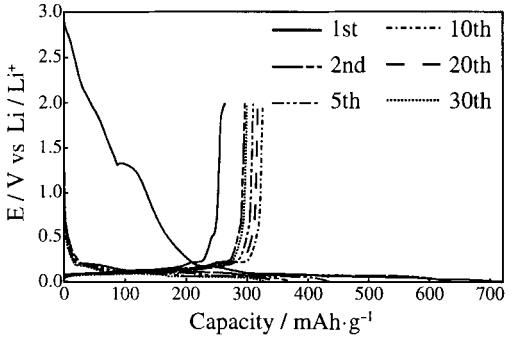

Figure 3. Reduction / oxidation cycles obtained with the binder-free graphite electrode (artificial graphite, KS-25, 1.8 mg·cm^{-2} on Mo) in the LiCl-saturated $AlCl_3$ (60 mol%)–EMIC (40 mol%) melt containing 0.11 mol·dm^{-3} $SOCl_2$. The graphite electrode was reduced at first cycle in the rate of 0.5 C (0.28mA·cm^{-2}). The following reduction and oxidation were done in the rate of 0.2 C. The graphite electorode was not allowed to stand for anytime before charging and discharging. Electrolyte temp.: 20 ℃.

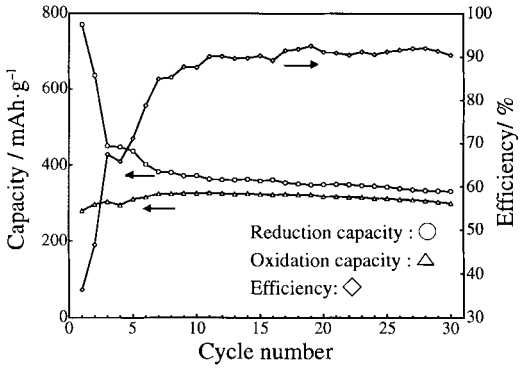

Figure 4. Changes in the reduction / oxidation efficiency and capacities for the reduction and oxidation of the binder-free graphite electrode. The experimental conditions are the same as those in Figure 3.

280mAh·g^{-1}, indicating the deintercalation of Li^+ from the graphite electrode. After the first cycle, the potential vs capacity curves for the reduction and oxidation showed clear three phase transitions between intercalation stages in the potential region from 0 to 0.2 V. The excess of capacity due to the formation of the SEI (around 0.3 V) decreased as the cycle progressed and the reduction capacity approached the theoretical capacity of graphite. On the other hand, the oxidation capacity increased as the cycles progressed. As a result, at the 30th cycle, capacities for the reduction and oxidation and reduction–oxidation efficiency reached 340, 310 mAh·g^{-1}, and 92%, respectively (Figure 4).

The intercalation and deintercalation could not be observed with the electrode composed of the mixture with various ratio of graphite and binder in the $AlCl_3$–EMIC–LiCl–$SOCl_2$ melts. The EMI^+ reductive intercalation (0.5–1 V) into the graphite electrodes has been also reported in the $AlCl_3$–EMIC melt in the absence of $SOCl_2$.[9] Judging from these results, the intercalation and deintercalation of Li^+ in the $AlCl_3$–EMIC–LiCl melt were realized using the binder-free graphite electrode and by the addition of $SOCl_2$. It can be considered that the removal of PVDF binder increases the wettability of the electrode surface by the melt and a large amount of Li^+ ion can intercalate and deintercalate easily, and that the addition of $SOCl_2$ produces the surface layers which prevent the EMI^+ reductive intercalation into the graphite as well as the extention of an electrochemical window.

The authors are grateful to Drs. K. Takeuchi, K. Ui, E. Yasukawa, and A. Kominato for useful discussions.

References

1 C. S-Kelley and R. T. Carline, *J. Electrochem. Soc.*, **141**, 873 (1994).
2 J. Fuller, R. A. Osteryoung, and R. T. Carlin, *J. Electrochem. Soc.*, **142**, 3632 (1995).
3 N. Koura, K. Iizuka, Y. Idemoto, and K. Ui, *Electrochemistry*, **67**(6), 706 (1999).
4 N. Koura, H. Tsuiki, N. Terakura, Y. Idemoto, F. Matsumoto, K. Ui, K. Yamada, and T. Mitate, *Hyomen Gijutsu*, **52** (1), 143 (2001).
5 D. Aurbach, B. Markovsky, I. Weissman, E. Levi, and Y. Ein-Eli, *Electrochim. Acta*, **45**, 67 (1999).
6 Z. Jiang, M. Alamgir, and K. M. Abraham, *J. Electrochem. Soc.*, **142**(2), 333 (1995).
7 J. Fuller and R. T. Carlin, *Electrochem. Soc. Proceeding*, **7**, 372 (1996).
8 T. Ohzuku, Y. Iwakoshi, and K. Sawai, *J. Electrochem. Soc.*, **140** (9), 2490 (1993).
9 R. T. Carlin, J. Fuller, W. K. Kuhn, M. J. Lysaght, and P. C. Trulove, *J. Appl. Electrochem.*, **26**, 1147 (1996).